International Journal of Recent Technology and Engineering (IJRTE)
ISSN: 2277-3878 (Online), Volume-8 Issue-4, November 2019

Numerical Analysis of Turbulent Flow over a 2-D Prolate Spheroid

Channabasav, Sharanappa Godignur

Abstract*: Recently external flow over body creates more interest of study because flow characteristics are dominated by complex phenomenon like separation and transition.in this paper turbulent flow over a 2-D prolate spheroid (6:1) is consider for analysis. Generation of surface grid around prolate spheroid by using grid generation code MESHGEN. Laminar and turbulent Flow past given geometry is simulated by Navier-stoke code RANS3D by second order upwind scheme for convective flux discretization by k-ε model for different Reynolds number, angles of attack .It is observed that the value of drag coefficient is lower than that of a cylinder due to its more streamlined contour. The variation of C_d was steeper in the laminar range than the turbulent range due to the effects of viscous forces being greater in laminar flow.

Keywords: 2-D turbulent flow, External flow, prolate spheroid, Numerical analysis, Navier stoke RAN3D code.

I. INTRODUCTION

A Prolate Spheroid is a spheroid in which the polar axis greater than diameter.Prolate spheroids are long along a line, whereas spheroids are contracted. The prolate spheroid is generated by rotation of an ellipse about the major axis. Prolate spheroid shaped balls are used in several sports, such as in Rugby, American Football, Canadian Football etc. Many simplified models of submarines, underwater vehicles, airships have a shape which can be described as prolate spheroid with different aspect ratios (8 :1, 6 : 1 or 3 : 1).

Though prolate spheroids are geometrically simple, the flow characteristics are dominated by complex phenomenon like separation and transition. The flow separation from the leeward side of the spheroid rolls up to form strong primary vortex on either side of the spheroid which reattaches on the plane of symmetry. The primary vortex is accompanied by a secondary vortex which separates and reattaches close to the wall surface. At zero angle of incidence the flow can be treated as two-dimensional axisymmetric flow, whereas for non-zero angle of incidence, favourable pressure gradient is prevalent on the windward side and adverse pressure gradient on the leeward side along the flow axis. Circumferentially the pressure gradient changes as we move from the front to the aft region. Several implementation and analysis have been reported for surface pressure and skin friction coefficient, profiles of mean velocity components and turbulent stresses and also details of the separated region at various angles of attack for Reynolds number Re = 4.5 $\times 10^6$.

Manuscript published on November 30, 2019.
* Correspondence Author
Channabasav*, School of Mechanical Engineering, REVA UNIVERSITY, Bangalore, India.
Dr Sharanappa Godignur, School of Mechanical Engineering, REVA UNIVERSITY, Bangalore, India. Email: Channabasav@reva.edu.in

II. SCOPE OF WORK

The geometry of a Prolate Spheroid is quite simple to generate but the flow past this simple geometry is often associated with very complex phenomena like the simultaneous presence of flow separation and laminar to turbulent transition. Several measurement and numerical simulations are reported on surface pressure, skin friction coefficient, profiles of turbulence quantities and also details of separated regions at various angles of attack. The present project work emphasizes mainly on:

- Generation of appropriate surface and volume grid for the ellipse as well as around a prolate spheroid using the in-house grid-generation code MESHGEN.
- Understanding the Navier Stokes code RANS3D for simulation of simple 2D laminar and turbulent flows like flow in a lid driven cavity, flow past aerofoil, etc.
- Simulation of 2D laminar and turbulent flow past an ellipse having the ratio of their axes as 6:1 for different Reynolds Number based on the major axis as the characteristic length, for different angles of attack, for variation convective flux discretisation steps and for variety turbulence schemes as well.
- 2D Turbulent flow simulation for flow past the same prolate spheroid for different Reynolds Number, angles of attack, flux discretisation schemes and also to study the effect of different turbulence models for turbulent flow situations and validate against reliable measurement data.

III. NUMERICAL GRID GENERATION

Generation of smooth body fitted grids with approximate orthogonality at the boundaries is practically the first step towards the accurate numerical solution of fluid flow equations. The present grid generation algorithm MESHGEN involves the solution of the elliptic type Poisson equations at a coarse level, followed by simple Bi-Cubic interpolation from the coarse to a finer level.

The 2D curvilinear grid with 561 nodes along the wall normal and 101 nodes along the circumferential direction, generated using FORTRAN code MESHGEN is shown in Fig. 1

Where the length of the major axis is assumed to be unity and the minor axis length is 1/6; the far field boundary for the C topology is assumed to be at a radius of 10 units for the curved inflow portion and the remaining part measuring 20 units is horizontal parallel to x direction.

The two dimensional C grid generated for the present problem is shown in Fig.1, where the wake portion at the inner boundary is rapped on itself as required in a C topology of the curvilinear grid. In order to obtain better resolution of the wall boundary layer.

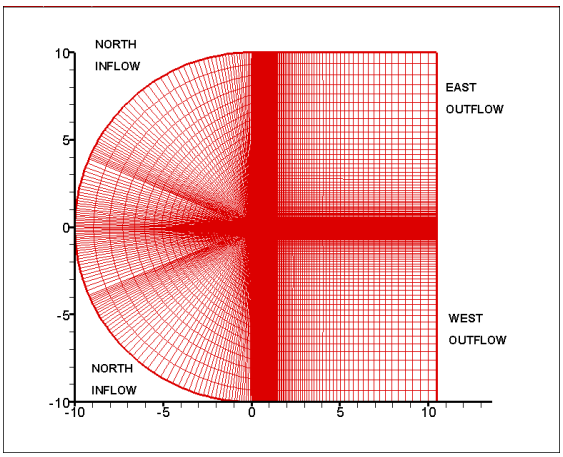

Fig.1 Axisymmetric 2D Grid with C topology around an Ellipse (Major to Minor axis = 6:1)

IV. MATHEMATICAL MODELING OF FLUID MOTION

The governing equations for unsteady three-dimensional incompressible turbulent flow in non-orthogonal coordinates using Cartesian velocities components, may be written in a generalized form of a scalar transport equation. The general structure of this equation represents the principal transport process for any passive scalar ϕ in three parts according to the mechanism of transport viz., convective ($C_{i\phi}$), diffusive ($D_{i\phi}$) and source components (S_ϕ).

A. General Transport Equation

$$\frac{\partial}{\partial t}(\rho\phi) + \frac{\partial}{\partial x_i}(\rho u_i \phi) = \frac{\partial}{\partial x_i}\left(\Gamma_\phi \frac{\partial \phi}{\partial x_i}\right) + S_\phi \qquad (1)$$

The convective transport again consists of two parts – (i) the local (the first term on LHS due to the unsteadiness of (ϕ) and (ii) the convection of ϕ through the velocity field (the second term on LHS). The third term on LHS represents the transport of ϕ due to diffusion, controlled by the generalized gradient hypothesis. The right hand side of the equation basically represents the sources or sinks (S_ϕ) per unit volume which, according to the conservation principle, is equal to the net balance of convective and diffusive fluxes of ϕ entering and leaving the faces of an elemental control volume. The physics of the flow is thus represented by the six coupled partial differential equations representing the conservation of mass, momentum components and two different turbulence scalars. All these six equations governing the transport processes and their corresponding convective ($C_{i\phi}$), diffusive ($D_{i\phi}$) and source (S_ϕ) components. where ' i ' is used as a summing index over i = 1,2 and 3 along the three spatial directions (x_1,x_2,x_3) on the computational domain . In order to determine the spatial and temporal field of V_1,V_2,V_3, p , k and ε , for any turbulent incompressible flow problem, one needs to solve these coupled nonlinear equation system – continuity for pressure (p), three velocity components (V_1,V_2,V_3) , turbulent kinetic energy (k) and turbulence dissipation (ε).

B. Finite Volume Equation:

The convective ($C_{i\phi}$) and diffusive ($D_{i\phi}$) fluxes computed according to the discretization scheme used, the conservation of fluxes in the form of a quasilinear equation for the respective flow variable solved for. The source terms are often non-linear and in order to enhance the numerical stability, the source terms for the steady state equations are linearized as:

$$\int JS_\phi \, dx_1 dx_2 dx_3 = SU^{steady} + \phi_P SP^{steady} \qquad (2)$$

Replacing the different fluxes and the source terms for the spatial derivatives and treating the temporal derivative in a simple first order backward difference form, the flux balance equation can be recast into the following quasilinear form.

$$\Delta V\left(\frac{\phi_P^{n+1} - \phi_P^n}{\Delta t}\right) + \left(\sum A_i - SP^{steady}\right)\phi_P^{n+1} = \sum_i A_i \phi_i^{n+1} + SU^{steady} \qquad (3)$$

Equation (3) simplifies further to the following form:

$$\left(\sum A_i - SP\right)\phi_p^{n+1} = \sum_i A_i \phi_i + SU$$

$$A_P\phi_P = A_W\phi_W + A_E\phi_E + A_S\phi_S + A_N\phi + A_B\phi_B + A_T\phi_T + SU \qquad (4)$$

Where,

$$SU = SU^{steady} + \Delta V . \phi_p^n / \Delta t$$

$$SP = SP^{steady} - \Delta V / \Delta t$$

The coefficient A_i represents the combined effect of convection and diffusion at the six faces of the cell denoted by the relevant directional suffices and SU and SP are the components of the linearized source term $S_\square$. The detailed derivation of Equation 4.3 expressing A_i as a function of cell face projection areas, velocity and diffusion coefficient at cell faces and variable values at the cell center is given elsewhere. The transformation of continuity equation to an equation of pressure-correction described in the following section is not that straightforward.

C. Boundary conditions:

Inflow: The values of all dependent variables are normally known at inflow boundaries and prescribed accordingly.

Outflow: Outflow boundaries far downstream with no reverse flow so that the results in the region of interest is practically insensitive to the treatment at outflow boundary. The usual practice is to extrapolate the field values at outflow from upstream neighbors in the interior of the computation domain.

Symmetry: The conditions to be satisfied at an axis or plane of symmetry are of zero flux across the plane or axis in question.

The convective fluxes are reduced to zero through prescription of zero convective coefficients and the diffusive fluxes are explicitly forced to zero.

Rigid Walls: All kind of diffusive fluxes at the wall are also set to zero. The wall shear effect is simulated through appropriate source terms in the momentum equations.

Cut Boundaries: two overlapping control volumes are provided on either side of the cut boundary and the value of the flow variables in these overlapping control volumes are transferred from the running solution of the adjacent domain.

D. Simulation:

computational results for (i) two dimensional laminar and turbulent flow past an ellipse for which the ratio between the major and minor axes is 6:1 and the computations have been carried out for different flow Reynolds number and also for different angles of attack.

All the computations use the Reynolds Averaged Navier Stokes solver (RANS3D) for unsteady incompressible flows. The flow solver is provided with five different convective flux discretization schemes and six different turbulence models. However for the present computation, two different schemes viz., and first order accurate pure upwind for the test runs and the second order accurate Linear Upwind has been used for discretization of convective flux in the final computations. Regarding turbulence model, the standard k-εmodel of Launder and Spalding [14] with logarithmic wall functions and also the low Reynolds number version of k-ε model, proposed by Chien [4] have been used for the present computations. .The Chien turbulence model which is used in all the 2D turbulent flow computation, constructs special exponential damping function, which allow the eddy viscosity to reduce from its local turbulence-dependent value in the boundary layer to zero on the wall. The objective of these computations is mainly to assess the performance and accuracy of the RANS3D code, for prediction of turbulent flow past a 6:1 ellipse as well as flow around a 6:1 prolate spheroid.

V. RESULT AND DISCUSSION

A. Two dimensional Flow Pattern around Ellipse:

Figs.2 (a) to (c) show the particle traces or streamlines plotted using the Tecplot360 software, based on the computed velocity vectors for the flow past ellipse (Re = 1000) at 3 different angles of attack. In each case, the flow is observed to hit the ellipse at the so-called front stagnation point near the nose and divided into two steams – one along the upper and the other along the lower surface of the ellipse. Further the stagnation point moves upwards or downwards from the leading edge as the angle of attack changes to negative or positive values respectively. We see from the images that follow that as the angle of attack increases, the separation bubbles move upwards along the direction of increase of angle. The bubble appears to elongate with an increase in the angle of attack.

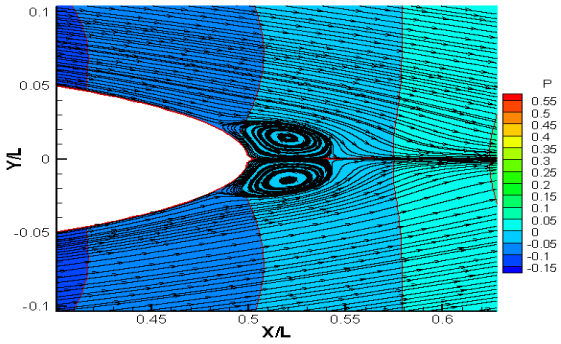

(a) $\alpha = 0^o$

The direction in which the angle is being increased shows a trait such that the bubble in that region is larger than the corresponding bubble in the opposite region. In our case as the angle of attack increases the separation bubble on top of the spheroid appears to be grow bigger than the one on the bottom of the spheroid. However in certain cases, it may be seem as though no separation is taking place. This could be due to unsteady flow and as the flow here is assumed to be steady.

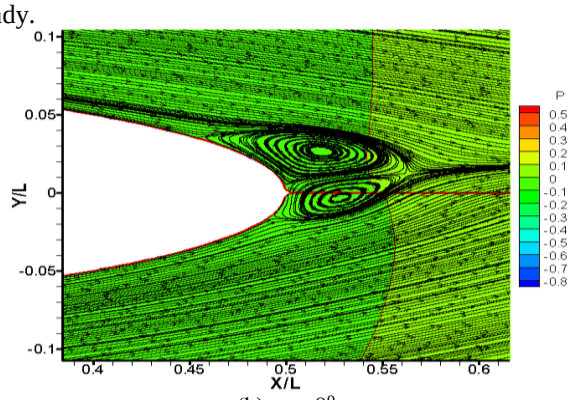

(b) $\alpha = 8^o$

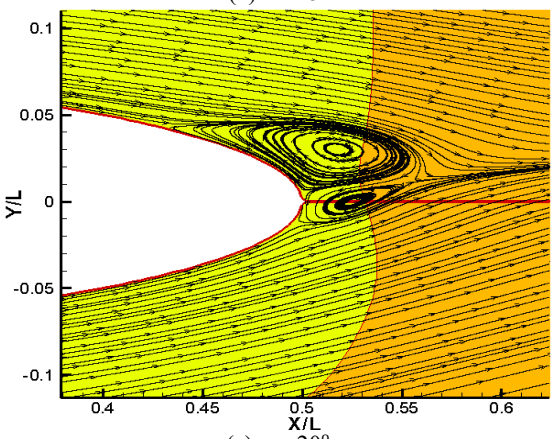

(c) $\alpha = 20^o$

Fig 2: Streamlines and pressure contours showing vortex formation at the trailing end of the spheroid at Re = 1000.

B. Surface Pressure and Skin Friction Coefficients for 2D Flow past Ellipse:

The variation of surface pressure coefficient (C_p) and skin friction coefficient (C_f) along the upper surface of the ellipse is shown in Fig. 3(a) to (d) for different values of Re varying between 10 and 1000 in the laminar regime and above 10^5 in the turbulent regime. The static pressure at the front stagnation point is quite high for a very low value of Re (=10)

since the viscous force has a strong influence on the pressure field, but as the value of Re increases the front stagnation point pressure tends to a value of unity as per the Bernoulli's equation balancing the pressure against the dynamic head. Along the curved body, the flow accelerates due to the curvature and hence the pressure tends to go down and reaches a negative maximum near θ equal to about 180 degrees where θ is measured from the front stagnation point. Further downstream the pressure is recovered once again when the flow decelerates due to the curvature of the body towards the trailing edge. Only beyond Re= 250 the flow separates at a point very close to the trailing edge and the skin friction coefficient changes the sign from positive to negative. In the mid region of the ellipse, the value of C_f is very close to that of a flat plate at the same Reynolds number. The flow separation in case of ellipse, before the rear stagnation point.

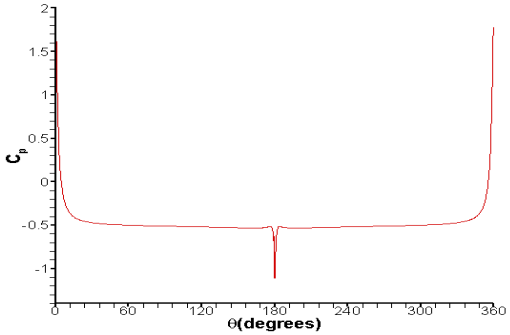

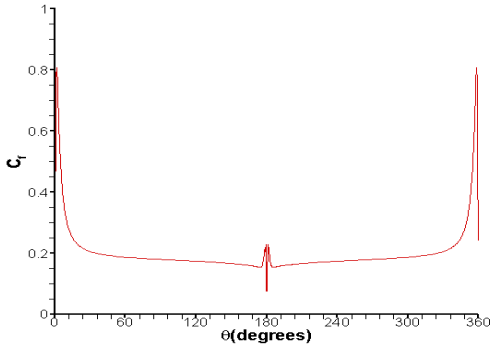

a) Re=10

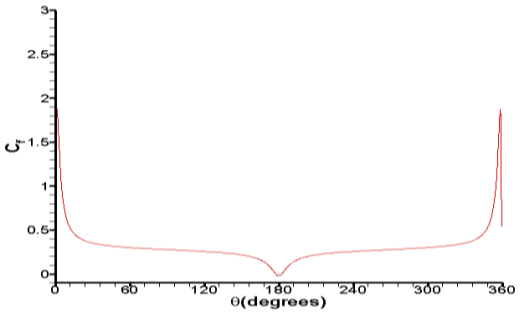

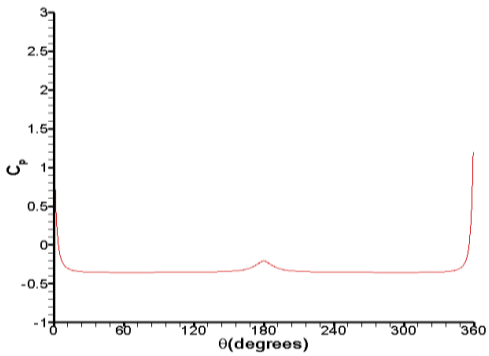

b) Re=250

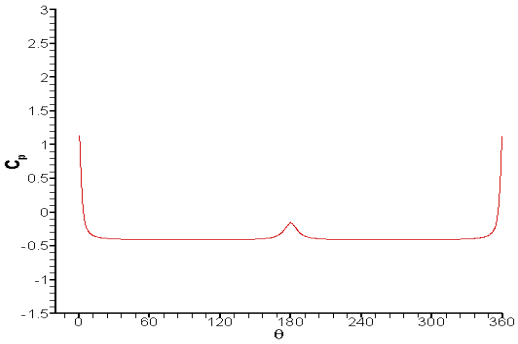

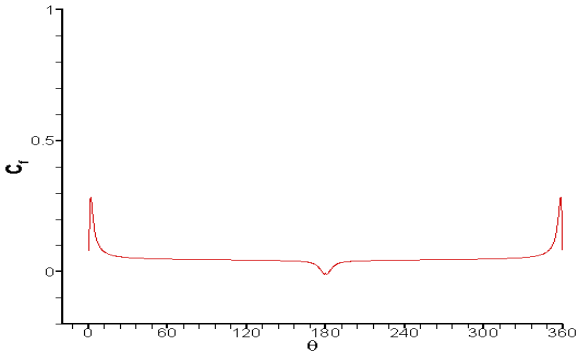

c) Re=1000

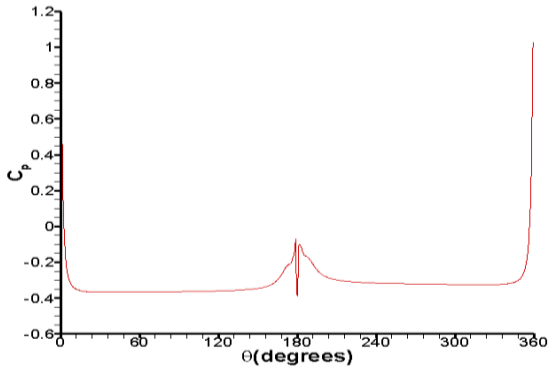

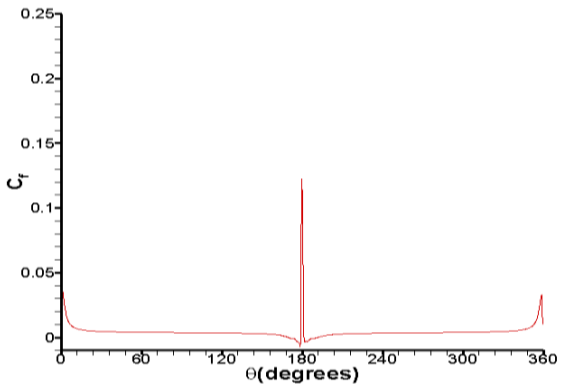

d) Re=10^5

Fig. 3 Variation of surface pressure and skin friction for various Reynold's number

C. Pressure Field and Flow Pattern around the Ellipse:

The below figures show a show the pressure contours and the streamlines at the trailing edge of the ellipse for Reynold's number that varies from laminar to turbulent. We observe in fig.4 that in the laminar flow the vortices do not start to form at the trailing edge till the Reynold's number reaches about 500. The vortices appear to elongate as the Reynold's number increases till it reaches 1000. At Re= 1000, the vortices seem to form very distinctive pattern. The pressure too appears to gradually increase as the Reynold's number increases.

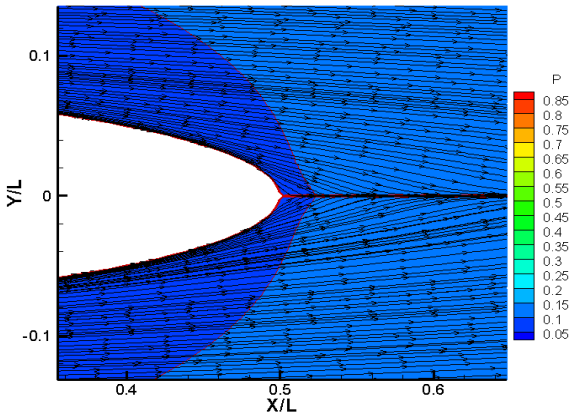

a) Re=250

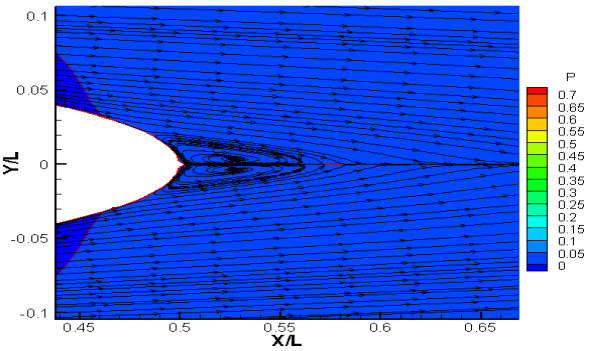

b) Re=500

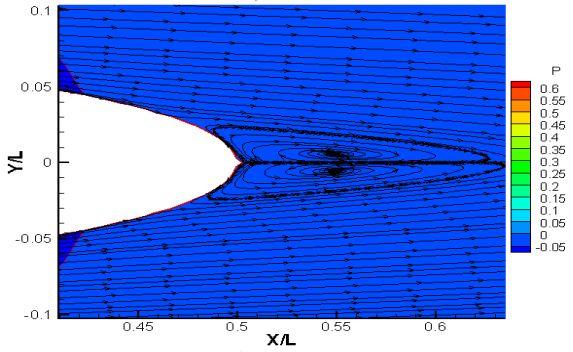

c) Re=750

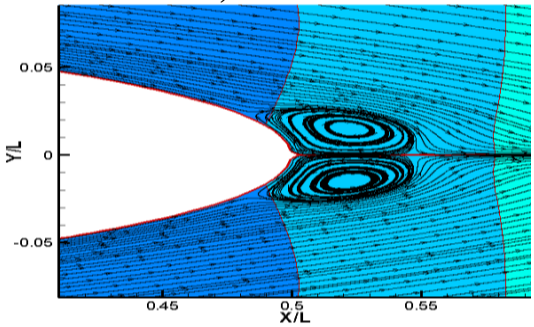

d) Re=1000

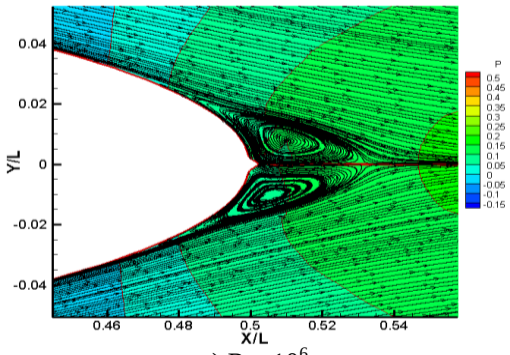

e) Re=10^6

Fig. 4 Pressure contours and flow pattern at the trailing edge of an ellipse for Reynolds numbers in the and laminar and turbulent range

D. Variation of Drag Coefficient with Reynolds number:

The below figures compares the variation of the coefficient of drag with change in Reynold's number. The Graph shows that in the laminar region the change in the value of C_d is more drastic than in the turbulent region. This could be due to the fact that in the laminar region the viscous forces dominate the flow pattern over the inertial forces. In turbulent flow cases the flow is more dominated by inertial forces and hence the value of C_d is more stable over a wide range of Reynold's numbers. Also the values of C_d appears to be lower in turbulent flow than in laminar flow. The Coefficient of lift C_l too was computed to be very small. This was as expected since lift is theoretically zero for this symmetric geometry facing a flow at zero angle of attack. The drag observed for an ellipse is much less than that of a cylinder because the drag on a bluff body like that of a cylinder is much higher compared to a more streamlined body like that of an ellipse.

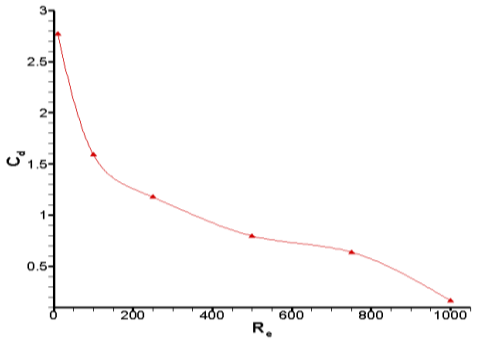

a) Laminar flow

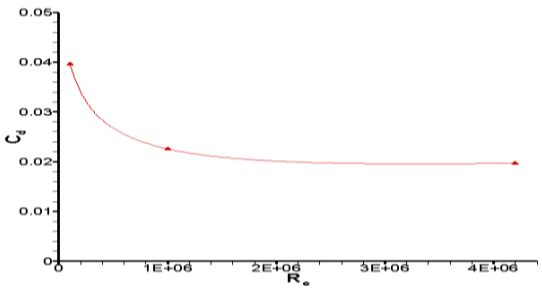

b) Turbulent flow

Fig. 5 Variation of Drag coefficient with Reynold's number for (a) Laminar flow (b) Turbulent flow

VI. CONCLUSION

- The grid generation code **MESHGEN** of NAL based on elliptic Poisson solver has successfully been used to generate multiblock curvilinear structured grid around an ellipse as well as around a prolate spheroid.
- The flow solution code **RANS3D** of NAL has been used successfully for simulation of laminar and turbulent flow past ellipse and turbulent flow past prolate spheroid at Re =4.12 Million The analysis uses the Second order accurate Linear Up winding scheme for convective flux discretization and both standard k- epsilon Chien's Low Re version of k-ε turbulence model.
- In two dimensional analysis for flow past a ellipse we observed that the value of drag coefficient is lower than that of a cylinder due to its more streamlined contour. The variation of C_d was steeper in the laminar range than the turbulent range due to the effects of viscous forces being greater in laminar flow.
- In three dimensional flow analysis we observed that the skin friction lines appeared to curve. This is due to the tendency of the flow to take the path of least resistance which may not always be a straight line. Also the surface pressure contours are similar to two dimensional flow.
- In future, advanced turbulence models with appropriate modeling of laminar to turbulent transition in the present RANS framework may be incorporated in the RANS3D code to generate more accurate results for Transitional Flow past Prolate Spheroid.

REFERENCES

1. D.KeithWalterd and DavorCokljat.A Three-Equation Eddy- Viscosity Model for Reynolds-Averaged Navier Stokes Simulations of Transitional Flow. Journal of Fluids Engg. 130, 2008.
2. Barber K. M and Simpson R. L. Mean Velocity and Turbulence Measurements of Flow around a 6: 1 Prolate Spheroid. AIAA Paper 91-0255, 1991.
3. Rupesh B. Kotapati-Apparao, Kyle D. Squires, and James R. Forsythe. Prediction of a Prolate Spheroid Undergoing a Pitch up Maneuver. American Institute of Aeronautics and Astronautics Paper 20030369, 2003.
4. C.J. Chesnakas and Simpson R.L. Measurements of the Turbulence Structure in the Vicinity of a 3-D separation. Journal of Fluid Engg. 118(2):268-275, 1996.
5. N. T. Hoang, Wetzel, T.G., and Simpson R.L. Unsteady Measurements over a 6:1 Prolate Spheroid undergoing a Pitch up Maneuver. American Institute of Aeronautics and Astronautics Paper 1994-01979, 35(6), 1994.
6. Weixing Yuan, Mahmoon Khalid, Jan Windte, Ulrich Scholz, and Rolf Radespiel.An Investigation of Low-Reynolds-number Flows past Airfoils. 23rd AIAA Applied Aerodynamics Conference, 2005.
7. P. Catalano and R. Tognaccini. RANS analysis of the low-Reynolds number flow around the SD7003 airofoil. Aerospace Science and technology, 15:615-626,2011.
8. C. Carton de Wiart and K. Hillewaert. DNS and ILES of transitional flows around a SD7003 using a high order Discontinuous Galerkin Method. Seventh International Conference on Computational Fluid Dynamics (1CCFD), 2012.
9. Fu. T. C., Shekarriz. A., Katz J., and Huang.T.T.The flow structure in the lee of an inclined 6:1 prolate spheroid Using and Unstructured Grid Method. Journal of the society of Naval Architects of Japan, 188:19,2000.
10. George S. Constantinescu, Hugo Pasinato, You-Qin Wang, James R Forsythe, and Kyle D. Squires. Numerical Investigation of Flow Past a Prolate Spheroid. Journal of fluids Engg. 124:904-910, 2002.
11. Zhixiang Xiao, Yufei Zhang, Jingbo Huang, Haixin Chen, and Song FU. Prediction of separation flows around a 6:1 prolate spheroid using RANS/LES hybrid approach. RESEARCH PAPER, School of Aerospace Engineering. Tsinghua University, Beijing, China, 23:369-382,2007.
12. Michael V. ol, Brian R. McAuliffe, Ernest S. Hanff, Ulrich Scholz and Christian Kahler, Comparison of Laminar Separation Bubble Measurements on a Low Reynolds Number Airfoil in Three Facilities. 35th AIAA Fluid Dynamics Conference and Exhibit, 6 - 9 June 2005, Toronto, Ontario Canada, AIAA 2005-5149
13. YongshengLian and Wei Shyy, Laminar-Turbulent Transition of a Low Reynolds Number Rigid or Flexible Airfoil, AIAA JOURNAL Vol. 45,No. 7, July 2007
14. B.E. Launder and D.B. Spalding, The Numerical Computation of Turbulent Flows, Computer Methods in Applied Mechanics and Engineering 3(1974) 269-289

AUTHOR PROFILE

Mr. Channabasav, Mr Chana Basavas working in REVA University School of mechanical engineering as Assistant professor with 3.5 years teaching experiences. He graduated from NMIT Bangalore and post graduated from MVJCE Bangalore in thermal power engineering. Author is active member in solar energy society of India (SESI) and his interested areas are computational fluid dynamics, IC engine, Solar Energy and attended 3 international conferences and published 2 international journal publications.

Dr. Sharanappa Godiganur has obtained his B.E degree in Mechanical Engineering from Gulbarga University, Master degree in Heat Power Engineering from KREC Surathkal. He pursued his doctoral degree in the area of Biodiesel application on Heavy Duty Diesel Engine from NITK Surathkal. He has teaching experience of over 30 years. He has published 28 technical papers in indexed and UGC approved Journals and has presented 25 technical papers in reputed National and International conferences. He has handled various subjects such as Basic Thermodynamics, Applied Thermodynamics, Fluid Mechanics, Turbomachinery, Refrigeration and Air conditioning, Strength of Materials, Cryogenics Engineering and Engineering Drawing. His areas of interests are Biofuel Application in IC Engines. Refrigeration and Air-conditioning, He is a life member of Institute of Engineers India (MIE),Indian Society of Technical education (MISTE), The Combustion Institute Indian Section and Energy & Fuel Users' Associations of India